Transient dynamics of eccentric double emulsion droplets in a simple shear flow

Sangkyu Kim
School of Mechanical Engineering, Purdue University, West Lafayette, Indiana 47907-2088, USA

Sadegh Dabiri*
School of Mechanical Engineering and Agricultural and Biological Engineering, Purdue University, West Lafayette, Indiana 47907-2093, USA

(Received 18 November 2016; published 19 October 2017)

We numerically examine the time-dependent behavior of double emulsions in a simple shear flow using finite volume and front-tracking methods. A single inner drop is initially located eccentrically to the outer drop. When the eccentricity is contained within the plane of shear, the inner drop experiences a "revolving" motion within the plane of shear, orbiting about the center of the compound drop while slowly moving outward. The inner drop eventually experiences a limit cycle, where no more outward movement occurs because the distance between the two interfaces is reduced to a thin liquid film for portions of the revolving cycle. In addition, eccentricity in the direction normal to the plane of shear is tested. In this case, the inner droplet undergoes a "drifting" motion, slowly moving perpendicularly to the plane of shear until only a thin layer remains between the two interfaces. Finally, the revolving and drifting motions are simultaneously observed when the in-plane-of-shear eccentricity is included in addition to the off-plane-of-shear eccentricity. The observed behaviors are not qualitatively affected by the inner to outer droplet radii ratio, and are preserved when $\mathrm{Re} \leqslant 5$, $\mathrm{Ca}_o \leqslant 0.1$, and $\mathrm{Ca}_i < 0.2$.

DOI: 10.1103/PhysRevFluids.2.104305

I. INTRODUCTION

A double emulsion droplet, also called a compound droplet or simply a double emulsion, is a nested liquid droplet system of three immiscible fluids. Because the innermost fluid is not making contact with the surrounding fluid, the usage of compound droplets as a predictable chemical delivery system has a significant impact in many fields including materials, pharmaceuticals, and microfluidics engineering. Furthermore, compound droplets can be used to model cells with nuclei. As such, researchers have focused on the stable production methods, steady-state configurations in various surrounding flows, stability associated with migration processes, and reliable breaking (release) mechanisms of compound droplets [1–3].

While the migration and deformation dynamics due to the surrounding flows are well known for single-phase droplets [4–7], the same cannot be said for compound droplets. Moreover, the literature on compound droplets is heavily centered toward production schemes and steady-state behaviors and is scarce on temporal response. Although the steady-state configurations of various droplets within given channels are vital in utilizing flow-focusing techniques and in controlling the breakup of droplets [8], the temporal evolutions and the feedback effects of droplets are equally important in many ways: first, as demonstrated for the case of simple droplets [9], in predicting the velocity and pressure feedback effects from already-produced droplets, which enables a stable compound droplet production mechanism; second, in understanding and predicting when and how the breakup of compound droplets may occur [10]; and third, in characterizing the stability of a given configuration of double emulsions [11].

*dabiri@purdue.edu

Torza and Mason [12] were the first to thoroughly investigate the interactions of three different phases and found various steady-state configurations. The focus of many following researchers have been with the fully engulfed compound droplet (meaning inner droplet does not make contact with the surrounding fluid) and the associated dynamics; Chen *et al.* [13–15] tested the extensional characteristics and breakup mechanisms when a single compound droplet is subjected to a shear flow by using both numerical and experimental tools. They found different steady-state regimes and breakup mechanisms for varying capillary numbers, radii ratio, and shear conditions. Interestingly, they found that the inner drop does not always suppress the deformation of the outer drop. Hua *et al.* [16] found similar steady-state deformations in two-dimensional (2D) and three-dimensional (3D) simulations with concentrically placed compound droplets. They also reported, through 2D numerical investigations, that eccentrically placed inner droplets in various positions all transitioned to the same concentric steady configuration under simple shear. Patlazhan *et al.* [17] also looked at two-dimensional compound droplets under shear flow by considering wall-confinement effects, and found nonmonotonic deformation as a function of the radii ratio and nonmonotonic steady-state orientation as a function of channel narrowing. By varying the capillary number and the ratio of the interfacial tension coefficients, Smith *et al.* found multiple breakup patterns when a compound drop is subjected to shear flow and then is allowed to relax [18].

Attempts have also been made to analytically solve for the flow inside and around a compound droplet; using Lamb's solution technique in spherical geometry [19], Taylor [20] predicted the deformation of a simple droplet under a simple shear. Following Taylor's work, Cox [21] found the deformation of a concentric compound droplet under a time-dependent flow. Following a similar formulation, Stone and Leal [22] solved for the velocity and pressure field inside and around a concentric and spherical compound droplet, then solved for the first-order deformation by matching the normal stress of spherical droplet to an interfacial tension stress due to a small deformation. They then verified and expanded upon the analytical work using the boundary integral method. Following the work from Stone and Leal, Qu and Wang [23] used the spectral boundary element method to verify the predicted deformation in extensional flows and investigated the effects of inner droplet placement; the inner drop was eccentrically placed in the plane of the surrounding extensional shear flow such that the geometry was symmetric in the direction normal to that plane. Because Lamb's solution is limited to spherical geometry, Sadhal and Oguz [11] utilized a bipolar coordinate system to solve for the Stokes flow of an eccentric compound droplet in a uniform flow. This eccentric solution was further investigated by Song *et al.* [24], who solved for the compound droplet in a cylindrical Poiseuille flow. In the last two studies, the compound droplet and the incoming flow were confined to an axisymmetric geometry and the eccentricity of the inner droplet was parallel to the imposed surrounding flow. Analyses performed by Stone and Leal, Qu and Wang, and Sadhal and Oguz have been extended by Mandal *et al.* [25], who included the effect of surfactant. They also solved for the migration of an eccentric compound drop under an axisymmetric flow using a bipolar coordinate system, and found that the eccentricity increases when the initial eccentricity is above a critical value. Additionally, the Lorentz reciprocal theorem was used by Haj-Hariri *et al.* to solve for the concentric compound drops in a general Stokes flow [26].

It is well known that simple drops and compound drops can break up in a shear flow [4,13,14] and also that the dynamics in shear flows can offer invaluable insight in understanding the dynamics in other flows [27]. In this light, the present study is aimed at understanding the temporal dynamics of double emulsion droplets in a simple shear flow. The response of compound droplets to other more complicated flows can be better understood by decomposing the imposed flows into a simple shear flow and other fundamental flows.

The main objectives of this work are threefold: first, to constitute the two fundamental motions—"revolving" and "drifting"—observed for an eccentric compound droplet exposed to a simple shear flow; second, to show how the two motions can be combined to collapse the motion of the inner droplet into a limit cycle; and third, to discuss the effects of the initial eccentricity, radii ratio, and the interfacial tension coefficients. In short, we demonstrate that the eccentricity of an inner droplet is always accentuated when all the fluids have the same viscosities and when the deformations are

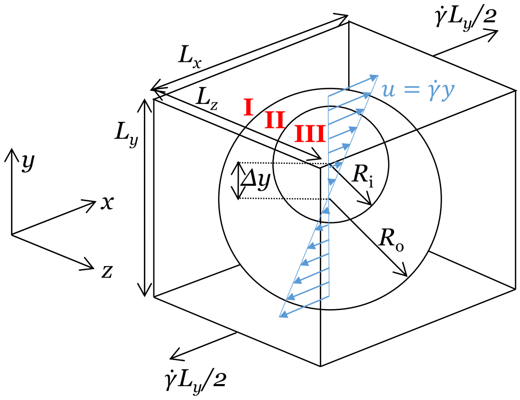

FIG. 1. Schematic of the computational domain with a single undeformed double emulsion droplet with eccentricity in the y direction. The outer drop is positioned at the center of the domain, whereas the inner drop can be placed away from the center if an eccentricity is wanted. Boundaries at $y = \pm L_y/2$ are moving with an equal and opposite velocities $\pm\dot{\gamma}L_y/2$. The origin is set at the center of the computational domain. Schematic is not drawn to scale.

small, meaning that the inner droplet always moves toward the outer interface until only a thin film remains between the inner and outer interfaces.

II. GOVERNING EQUATIONS

We consider a compound droplet that is suspended in a shear flow as shown in Fig. 1. With the origin defined at the center of the computational domain, the background shear is defined by $\mathbf{u}_\infty = \dot{\gamma} y \hat{\imath}$ and is imposed by the the velocity boundary condition at the top and bottom walls (i.e., walls normal to the y direction) that are driven in the $\pm x$ direction with equal and opposite velocities $\pm\dot{\gamma}L_y/2$. The other boundaries are periodic. The different and immiscible fluid phases are incompressible and Newtonian with densities ρ^Φ and viscosities μ^Φ, where Φ ranges from I to III. We let phase I denote the surrounding fluid, II the outer droplet, and III the inner droplet. We define the interface between phases I and II as the outer interface and that between II and III as the inner interface. We also define the interfacial tension coefficients, σ_i and σ_o, for the inner and outer interfaces. The governing equations for the unsteady and incompressible viscous flows are given by the Navier-Stokes equations,

$$\rho^\Phi\left(\frac{\partial \mathbf{u}}{\partial t}+\mathbf{u}\cdot\nabla\mathbf{u}\right) = -\nabla p+\nabla\cdot(2\mu^\Phi\mathbf{D})+\int_i \sigma_i\kappa_i\delta(d_i)\mathbf{n}_i dA_i + \int_o \sigma_o\kappa_o\delta(d_o)\mathbf{n}_o dA_o, \quad \nabla\cdot\mathbf{u} = 0, \tag{1}$$

where $\mathbf{u}$ is the velocity vector, p is the pressure, $\mathbf{D} = \frac{1}{2}[\nabla\mathbf{u} + (\nabla\mathbf{u})^T]$ is the strain rate tensor, κ_i and κ_o are the curvatures associated with the respective interfaces, δ is the Dirac δ function, d_i and d_o are the distances from the respective interfaces, $\mathbf{n}_i$ and $\mathbf{n}_o$ are the unit normal vectors at the interfaces, and dA_i and dA_o are the area elements at the interfaces. The effect of gravity is not considered.

Let R_i and R_o be the initially undeformed radii of the inner and outer droplets; then we can characterize the flow with the following nondimensional parameters:

$$\text{Reynolds number: Re} = \frac{\rho^\text{I}\dot{\gamma}R_o^2}{\mu^\text{I}}, \tag{2}$$

$$\text{Capillary numbers: Ca}_i = \frac{\mu^\text{I}\dot{\gamma}R_i}{\sigma_i}, \quad \text{Ca}_o = \frac{\mu^\text{I}\dot{\gamma}R_o}{\sigma_o}, \tag{3}$$

$$\text{Radii ratio: } k = \frac{R_i}{R_o}, \tag{4}$$

$$\text{Interfacial tension coefficient ratio: } \beta = \frac{\sigma_i}{\sigma_o}. \tag{5}$$

In this work, we look at $\mathrm{Re} = O(1)$, $k = 0.4$–0.6, $\mathrm{Ca} = O(0.01)$–$O(0.1)$, and $\beta = 0.1$–1. Because of the low Reynolds number that is typically associated with double emulsions, the ratio of the densities does not play an important role. On the other hand, the ratio of the viscosities does, but we do not look into its effect at this time. Therefore, all the three phases are chosen to have uniform densities and viscosities.

Additionally, we quantify the deformation of both the inner and outer droplets by using

$$\chi = \sqrt{I_{\max}/I_{\min}}, \tag{6}$$

the square root of the ratio of the largest and smallest eigenvalues of the second moment of inertia tensor, which in turn is quantified as [28]

$$I_{lm} = \frac{1}{\mathcal{V}} \int_{\text{droplet}} (x_l - x_{lc})(x_m - x_{mc}) dV. \tag{7}$$

Here, $\mathcal{V}$ is the volume of a given droplet (whether it be inner or outer), x_l and x_m are the general coordinates, and x_{lc} and x_{mc} are the droplet's centroids in the l and m directions. The deformation χ has been shown to correspond to the aspect ratio of a droplet for a small deformation [29] and can be cast into Taylor deformation number [30] for the inner and outer interfaces as

$$D_i = \frac{L_i - B_i}{L_i + B_i} = \frac{\chi_i - 1}{\chi_i + 1}, \quad D_o = \frac{L_o - B_o}{L_o + B_o} = \frac{\chi_o - 1}{\chi_o + 1}, \tag{8}$$

where L and B are the instantaneous major and minor axes of the respective interfaces.

III. NUMERICAL IMPLEMENTATION

We use finite-volume method on a three-dimensional staggered grid to discretize and solve for the numerical solution of the unsteady Navier-Stokes equations. We compute the advective terms using the quadratic upstream interpolation for convective kinematics (QUICK) scheme [31] and solve for the pressure-velocity coupling using the projection method [32], which is numerically implemented using the Hypre library [33]. We represent the interfaces with unstructured grids using the front-tracking method [34]; the interfaces of the inner and outer drops are not allowed to make topological changes (e.g., break up or merge). This corresponds to the physical case of a dilute surfactant concentration that prevents the merging of the surfaces [35], yet does not affect the interfacial tension. Finally, we advance the solution in time with second-order explicit Euler method using Courant-Friedrichs-Lewy condition of 0.9.

First we perform a grid refinement test. The length scale is nondimensionalized by the diameter of the undeformed outer droplet and the time scale by the shear rate. A single compound droplet, initially undeformed with $R_o = 0.5$ and $R_i = 0.25$, is placed in the center of a shear-driven domain of size $L_x \times L_y \times L_z = 2 \times 2 \times 2$ with a shear rate of $\dot{\gamma} = 1$. The uniform viscosities and densities are chosen such that $\mathrm{Re} = 1.25$, and the interfacial tension coefficients are chosen such that $\mathrm{Ca}_i = 0.025$ and $\mathrm{Ca}_o = 0.05$. The inner drop's center is offset from that of the outer drop in the x direction by $R_o/4$. The domain is uniformly divided into 64^3, 128^3, and 256^3 grids, giving 16, 32, and 64 grids across the initially undeformed inner droplet diameter.

The comparison of Taylor deformation and inner droplet position relative to the outer droplet are shown in Fig. 2, where the local extrema in relative position are circled. The positions of the inner and outer droplets, $\mathbf{x}_i = (x_i, y_i, z_i)$ and $\mathbf{x}_o = (x_o, y_o, z_o)$, are computed by taking the center of mass of the respective phases, and the relative position is then acquired as $\mathbf{x}_i - \mathbf{x}_o$. We find a good agreement in the relative position of the inner droplet with 16, 32, or 64 grids across the inner drop diameter,

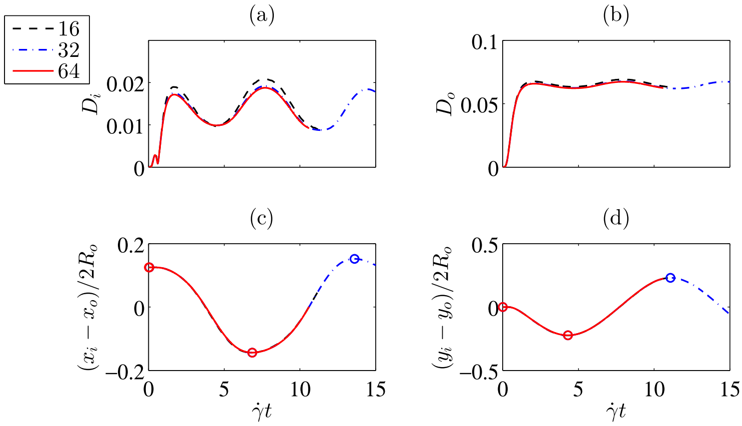

FIG. 2. Grid independency test with 16, 32, and 64 grids across the initial inner droplet diameter. (a) Inner drop Taylor deformation; (b) outer drop Taylor deformation; (c) normalized relative x position of inner drop; and (d) normalized relative y position of inner drop. The local extrema are noted with circles in panels (c) and (d).

and in the deformations with 32 or 64. The first local extrema are tabulated in Table I alongside a comparison of the relative position at the time when the first extremum occurs with coarse grid.

We notice an abrupt change in D_i for $\dot{\gamma}t < 1$, similarly noted by Chen *et al.* [14]. This initial jump seems to not have been caused by a specific treatment of the initial computational domain, as simulations with initially quiescent domain as well as simple shear profile domain both show this behavior. Rather, it seems to arise from the deformation of the outer droplet, and the resulting flow field inside. The outer drop's deformation in steady state or limit cycle behavior (which will be later described) matches well with Chen *et al.* [15] with 32 grids across the inner diameter, as shown in Fig. 3; a slight difference with $\mathrm{Ca}_o = 0.1$ likely arises because the stable configuration in our simulations was an eccentric compound drop, whereas Chen *et al.* looked at the deformation of a concentric compound droplet. The deformation with Ca_o matches better because the stable configuration in our simulations was a concentric configuration. The transition from eccentric to concentric configuration will be described later. Simple drop deformation from Rumscheidt and Mason [36] is also shown for comparison.

The difference due to grid spacing in the relative positions of the inner droplet is less than 1%, as shown in Table I. On the other hand, the deformation data show a close convergence between medium and fine grids. We therefore use 32 grids across the inner droplet for all remaining numerical calculations. Also for convenience, we refer to the center of mass of the inner and outer droplets as simply their positions. Because the positions of the droplets can vary depending on the starting configurations, we look at the relative position of the inner droplet to the outer droplet.

We also verify the validity of the code against the results from Hua *et al.* [16]. For this, the code is modified for 2D simulations, and cases 1, 2, and 3 outlined in Sec. 4.2.3 of Hua *et al.*

TABLE I. Grid convergence versus number of nodes across undeformed inner droplet diameter.

	Coarse (16)	Medium (32)	Fine (64)
First $(x_i - x_o)/2R_o$ extrema	−0.1440	−0.1441	−0.1438
$(x_i - x_o)/2R_o$ @ $t = 6.88$	−0.1440	−0.1441	−0.1438
First $(y_i - y_o)/2R_o$ extrema	−0.2242	−0.2233	−0.2284
$(y_i - y_o)/2R_o$ @ $t = 4.85$	−0.2242	−0.2232	−0.2228

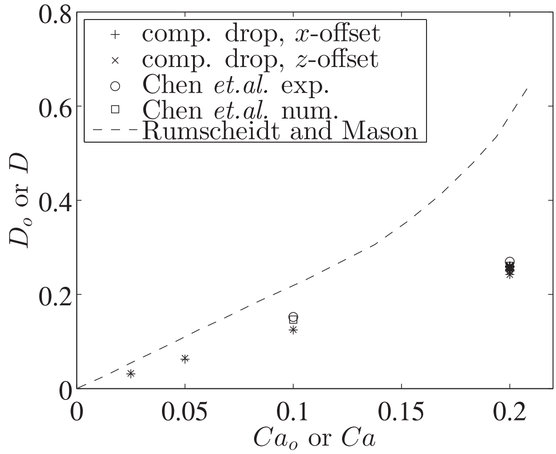

FIG. 3. Outer drop deformation with $k = 0.5$ with $\mathrm{Ca}_o = 0.025$–0.25. The deformation is averaged over time after a limit cycle behavior or steady state is reached, and compared against the compound drop results from Chen *et al.* [15] and simple drop results from Rumscheidt and Mason [36].

are tested; here, $\mathrm{Re} = 1$ and $\mathrm{Ca}_o = 0.25$ with $k = 0.5$. The inner droplet center is initially located at $(-1/4,0)$, $(-\sqrt{2}/8,\sqrt{2}/8)$, and $(0,1/4)$ relative to the outer droplet. As shown in Fig. 4, the interfaces at steady state show a good qualitative match with the results presented by Hua *et al.*

IV. NUMERICAL RESULTS AND DISCUSSION

A. Revolving and drifting of the inner droplet

We examine the effect of eccentricity by initially displacing the inner droplet in the x, y, and z directions by $R_i/2$. The Taylor deformation number and the relative position between the inner and outer droplets, $x_i - x_o$, $y_i - y_o$, and $z_i - z_o$, are shown in Figs. 5(a), 5(c) and 5(e) after nondimensionalization. The relative positions whose magnitude variations are on the order of 10^{-4}, which is an order of magnitude smaller than the grid spacing, are not shown. The absolute position

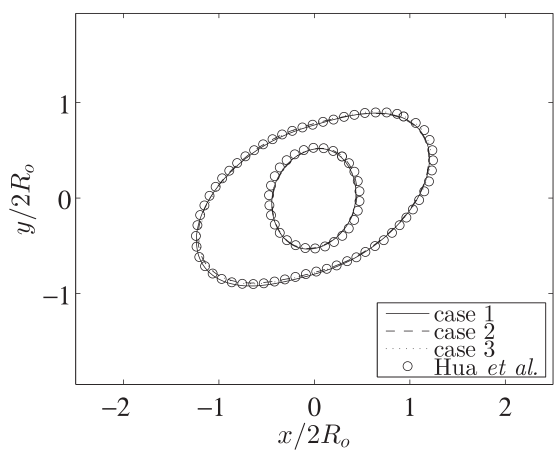

FIG. 4. Eccentric compound droplet in 2D at steady state. For the three cases simulated, the inner droplet centers relative to the outer droplet are initially located at $(-1/4,0)$,$(-\sqrt{2}/8,\sqrt{2}/8)$, and $(0,1/4)$. The final compound droplet configurations agree with those from Hua *et al.* [16].

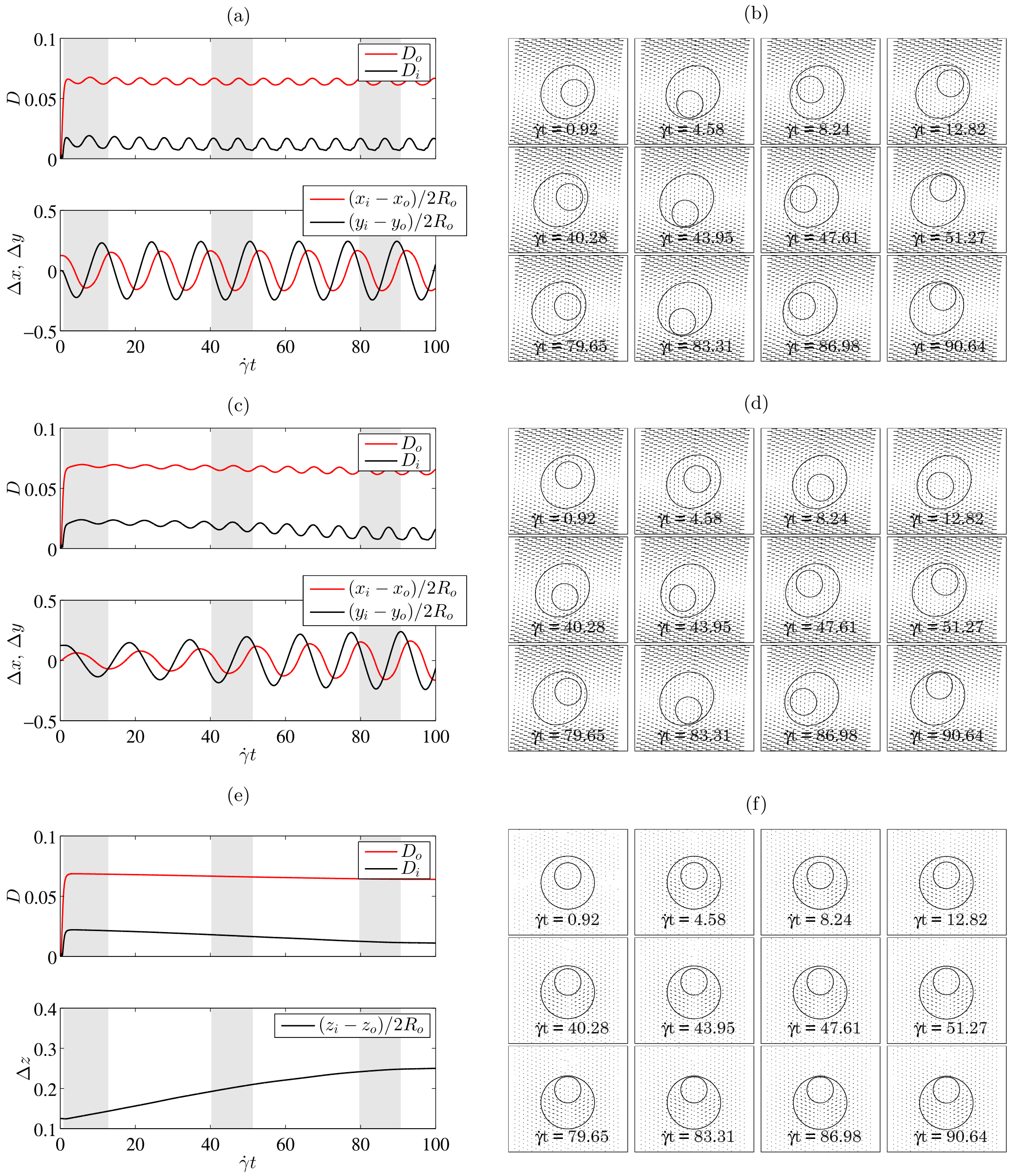

FIG. 5. Inner droplet deformation, position, shape, and the velocity vectors tangent to the viewing plane. Taylor deformation, nondimensional relative x, y, and z positions with initial eccentricity in the (a) x, (c) y, and (e) z directions are shown; xy plane view of the interfaces and the velocity vectors with eccentricity in the (b) x and (d) y directions; (f) xz-plane view of the interfaces and the velocity vectors, magnified $\times 2$ for visibility, with eccentricity in the z direction. The plane views (b), (d), and (f) are shown at times shaded in panels (a), (c) and (e).

of the outer drop, which is representative of the position of the compound drop as a whole, is not shown because the overall movement in the x and z directions is not meaningful due to the nature of the periodic domain and because there is no movement in the y direction.

The droplet positions, shapes, and the tangential velocity field at the midsection of the outer droplets are shown in Figs. 5(b), 5(d) and 5(f). The viewing planes are chosen to show the direction of the significant inner droplet movement, and the velocity magnitudes are multiplied twofold in Fig. 5(f) for visibility.

Two very distinct motions are readily observed: one where the inner droplet persists in a "revolving" motion in the xy plane (plane of shear) with almost no change in its z position (the direction normal to the plane of shear), and the other where there is no revolving motion but only a "drifting" motion in the z direction. The characteristics of revolving and drifting motions are further explained in the following subsections.

1. Revolving motion in the plane of shear

We observe a persistent circulatory movement of the inner droplet when it is eccentrically placed with x or y offset. Figures 5(a)–5(d) illustrate that the inner droplet migrates outward while orbiting about the center of the outer drop until a limit cycle behavior is reached; during the limit cycle, the inner drop continues to revolve about the center of the outer drop but is no longer able to move outward because the interfaces almost touch; the interfaces do not actually come into contact; and a thin liquid film forms for portions of the limit cycle. The trajectory of the inner drop in limit cycle resembles a slanted ellipse, and is described in more detail in Sec. IV A 3. Because of both the elongation of the outer droplet and also the slanted elliptical limit cycle, the inner droplet almost touches the outer droplet's interface for only parts of a revolving cycle; e.g., the two interfaces are not very close to each other at $\dot{\gamma}t = 86.98$ but are at $\dot{\gamma}t = 90.64$ in Fig. 5(d). This causes the outer drop's deformation to undergo "breathing," fluctuating at twice the frequency of the oscillation in the x and y positions.

The fact that the y-eccentricity case reaches limit cycle behavior when $\dot{\gamma}t \sim 100$ is not clear in Fig. 5(c) but can be realized from Fig. 5(d), since the interfaces are almost touching when $\dot{\gamma}t \sim 90.64$, implying no more outward motion. In fact, all cases were run until $\dot{\gamma}t = 200$ to ensure that the limit cycle has been reached, but only the range $\dot{\gamma}t = [0,100]$ is shown in Fig. 5. At first glance, it seems that the x-eccentricity case reaches limit cycle more quickly than the y-eccentricity case. This is reflective of the initial condition rather than the qualitative characteristic of the revolving motion: Since the movement of the inner drop in the x and y directions is coupled by the revolving motion, different initial x and y eccentricities serve as different initial conditions to the fundamentally identical outward orbiting motion. Figures 5(b) and 5(d) further show that having an initial x or y eccentricity in the inner droplet placement does not affect the final limit cycle, and Figs. 5(a) and 5(c) show that the offset positions and the Taylor deformations match well after limit cycles are reached.

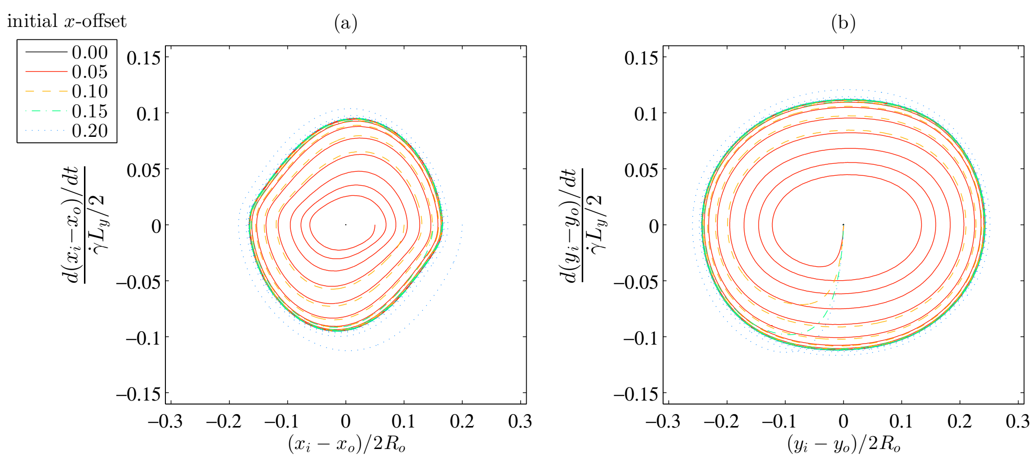

FIG. 6. Phase portraits of dimensionless relative (a) x velocity and (b) y velocity of the inner droplets vs the dimensionless relative position. The inner droplet is initially offset in the x direction with magnitudes noted in the legend.

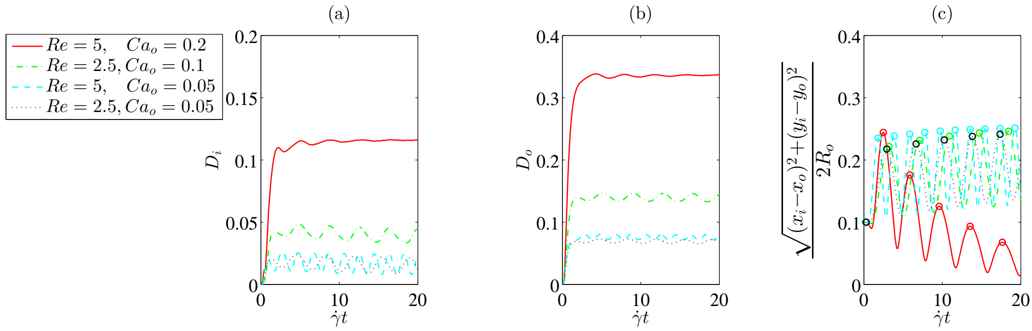

FIG. 7. The inertial effect on the revolving motion is investigated by increasing the shear rate with and without keeping Ca_o constant. Given an initial x eccentricity, (a) D_i, (b) D_o, and (c) normalized distance from the inner drop center to the outer drop center, with local maxima noted with circles, are shown. The reversal in the outward motion with $\mathrm{Re} = 5$ and $\mathrm{Ca}_o = 0.2$ is due to a large deformation in the outer drop.

Simulating multiple offsets in the x direction reveals that the revolving motion is ubiquitous and alike despite the varying degree of offsets and that the revolving motions starting with different initial eccentricity all collapse to the same limit cycle. This fact is illustrated in Fig. 6 by phase portraits of inner droplet's velocity versus position.

Based on the flow field inside a simple drop subject to a shear flow, a similar revolving motion of the inner droplet was assumed by Klahn *et al.* [10] in characterizing the escape mechanism of an inner droplet. However, their assumption was that a given inner droplet is bound to the concentrically elliptical streamlines that it was originally placed in, and therefore coalescence between multiple inner droplets was suggested as a means of escaping such a confinement. On the contrary, the results given here demonstrate that inner droplets are capable of moving radially outward without coalescence, so long as an initial offset in the plane of shear is realized. Chen *et al.* also reported a circulatory streamline inside the outer droplet but did not observe a revolving motion. We believe this is due to the much smaller Reynolds number they had ($\mathrm{Re} \sim 10^{-5}$), which would have retarded the amplitude increase of the eccentricity from the nearly concentric compound droplets they had.

The outward motion is driven by the pressure force and the shear stress and is not affected by the inertial effects as long as the deformations are small. The lack of inertial impact on the outward

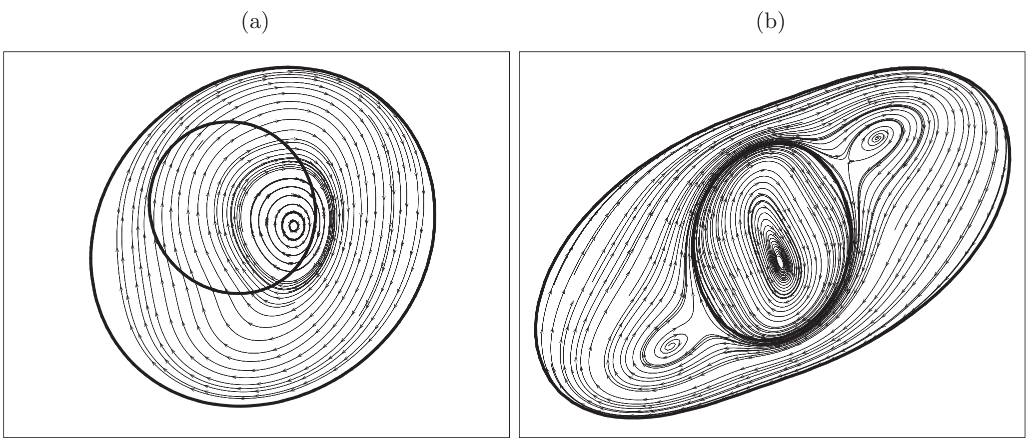

FIG. 8. The streamlines inside the compound droplet at the midsection with an initial x eccentricity with (a) $\mathrm{Re} = 5$ and $\mathrm{Ca}_o = 0.05$ after reaching limit cycle behavior and (b) $\mathrm{Re} = 5$ and $\mathrm{Ca}_o = 0.2$ after reaching steady state. The larger deformation creates recirculation zones in panel (b), making a steady state obtainable.

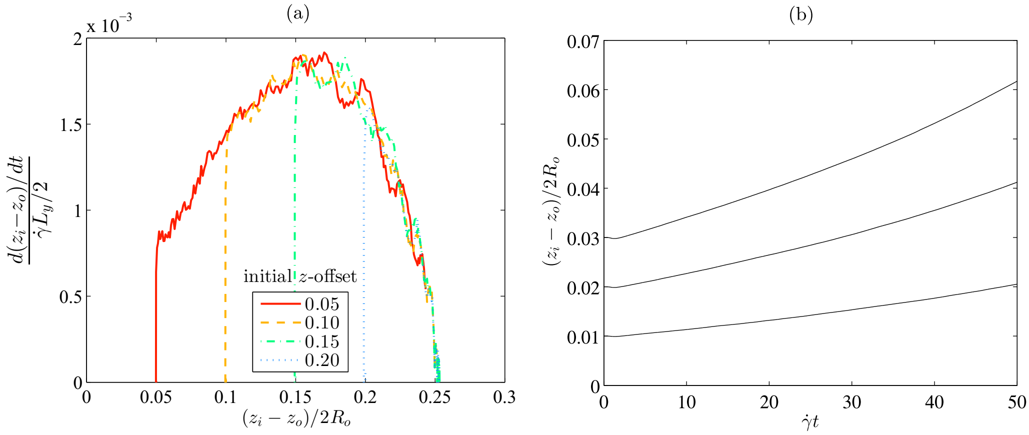

FIG. 9. (a) Phase portrait of dimensionless relative z velocity vs position of the inner droplet. The inner drop is initially offset in the z direction with the magnitudes indicated in the legend. (b) Dimensionless relative z-direction movement of the inner drop vs dimensionless time, given various initial offsets in the z direction.

motion can be seen by increasing the shear rate, as can be seen in Fig. 7. Even after increasing the Reynolds number by a factor of 4, the outward motion is preserved so long as deformations are controlled by simultaneously increasing the inner and outer interfaces' tension coefficients to keep Ca_o and Ca_i constant.

We do see a reversal in the outward motion when $\text{Re} = 5$ and $\text{Ca}_o = 0.2$. This is not an inertial effect but rather a deformation effect. This fact is well illustrated in Fig. 8: When the deformation of the outer drop is sufficient, recirculation zones are created inside the outer drop, creating a stable configuration. This transition of streamlines is similar to what was observed for a compound vesicle (a simple drop with a membrane and with a particle inner core) by Veerapaneni *et al.* when it underwent the transition from tank treading to tumbling [37]. The fact that the creation of recirculation zones within the outer drop contributes to a transition in dynamics was also found by Zhou *et al.*, who saw a nonmonotonic relationship between k and the time a compound drop takes to squeeze through a choke in a pressure-driven flow [38].

The critical capillary number for the transition from reaching limit cycle to reaching steady state lies between $0.1 < \text{Ca}_o < 0.2$, given that $\text{Ca}_i = 0.15$. The critical transition Ca_o depends on the deformation of the inner drop, i.e., on Ca_i and possibly k. Generally speaking, $D_o > D_i$, so there is little room left for examining the effect of increase in Ca_o past $\text{Ca}_o = 0.2$ before breakup occurs.

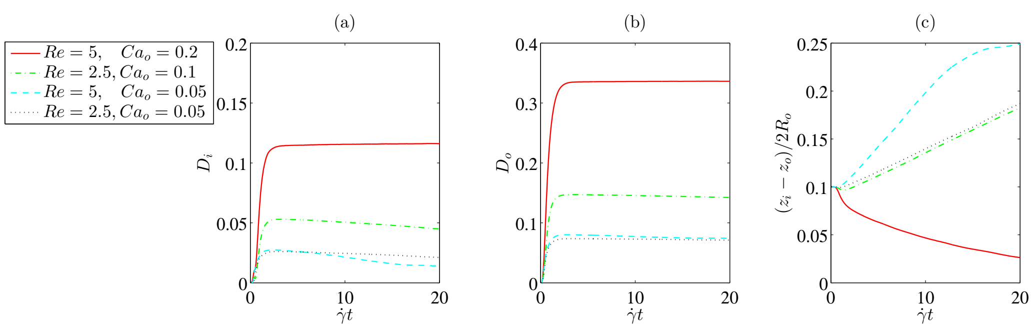

FIG. 10. The inertial effect on the drifting motion is investigated by increasing the shear rate with and without keeping Ca_o constant. Given an initial z eccentricity, (a) D_i, (b) D_o, and (c) normalized relative z position of the inner drop are shown. The reversal in the drifting motion with $\text{Re} = 5$ and $\text{Ca}_o = 0.2$ is due to a large deformation in the outer drop, as was the case in the revolving motion.

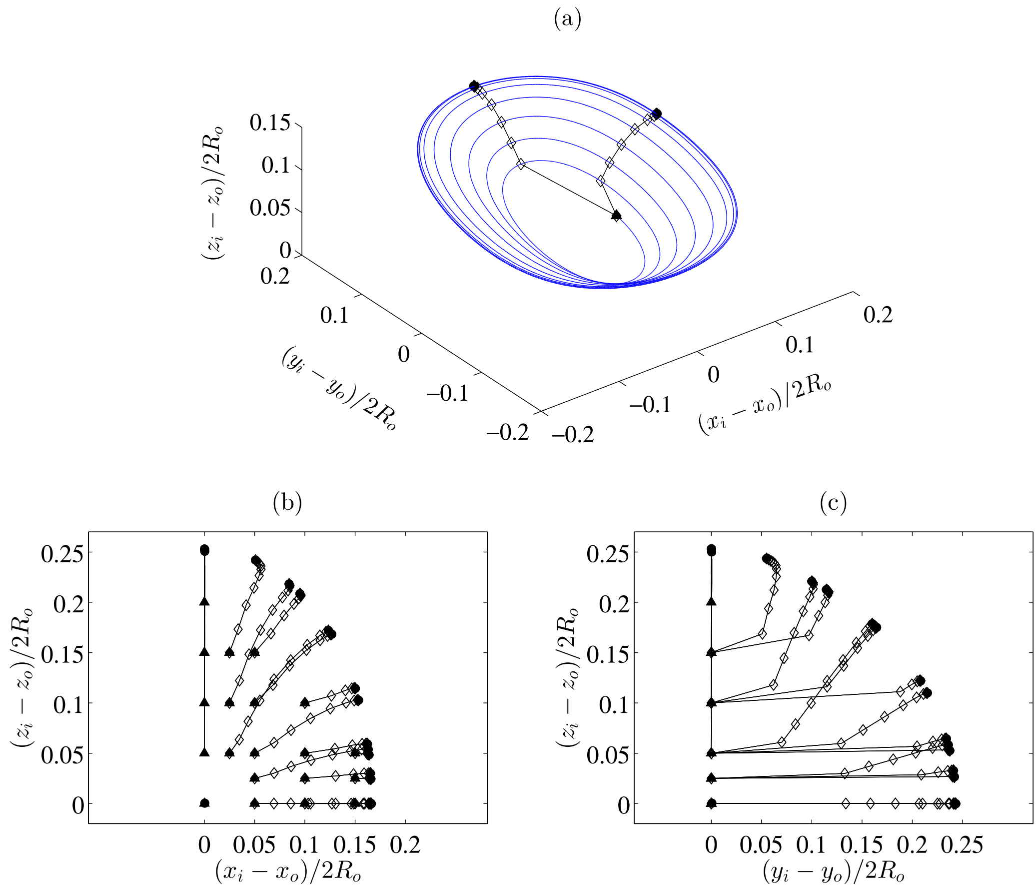

FIG. 11. Dimensionless (a) three-dimensional (3D) view of the migration path of the inner droplet initially placed at $(x,z) = (0.05,0.05)$ with $k = 0.5$. The two black lines represent how the (b) xz-plane view and (c) yz-plane view are acquired when various initial eccentricities are tested. The initial positions are marked by triangles. The open diamonds denote the local maxima in (b) x and (c) y positions such that only the outward component of the motion is shown from the combination of revolving and drifting motions. The global maximum in x or y (i.e., envelope of the limit cycle) is shown with filled circles.

The effects of Ca_o and Ca_i are discussed in more detail in Sec. IV C. The effect of k on the transition Ca_o is not quantified in this work, but its presence can be deduced from the fact that k affects the outer drop deformation [15] and creation of recirculation zones [37,38].

2. Drifting motion normal to the plane of shear

Unlike the pure revolving motion, the motion in the xy plane is negligible when the inner droplet is initially displaced in only the z direction. Rather, the inner droplet slowly drifts in the direction of the offset (which is the direction normal to the plane of shear), increasing in eccentricity until only a thin liquid film remains between the interfaces [see Fig. 5(e) and 5(f)].

Various offsets in the z direction all result in the same behavior, and the inner droplet always moves in the direction that increases the offset. Moreover, the drift velocities for different offset distances collapse into a single curve as shown in Fig. 9(a), where the initial z offsets are noted in the legend; the initial spikes are due to the computational domain being initially quiescent. The fact that all velocities collapse independently of the offset magnitude indicates that the drifting motion is a fundamental behavior of compound droplets in a shear flow; surprisingly, this collapse holds even for eccentricities that are on the order of the droplet radii. The time variation of the drifting motion with varying initial eccentricity is explicitly shown in Fig. 9(b).

As was the case with revolving motion, the drifting motion does not seem to be caused by inertial effects. As can be seen in Fig. 10, changing Re while keeping Ca_o and Ca_i constant results in increase in the z eccentricity. When Re is changed while not keeping the deformations constant, a decrease in eccentricity is possible. When that happens, the steady-state configuration that was previously shown in Fig. 8(b) is recovered. However, the disappearances of revolving motion and drifting motion need not be linked, as will be discussed in Sec. IV C.

3. *Combined motion*

The natural extension of the revolving and drifting motions is to characterize if specific initial configuration dictates the final configuration of the inner droplet. Because having the inner droplet offset in either the x or the y direction results in the same limit cycle, whereas having z offset results in a completely different motion, we look at various eccentric inner droplet placements in the xz plane.

The initial offset, outward migration path, and the final limit cycle behavior of the inner droplets are illustrated in Fig. 11. The initial positions are marked with filled triangles. The open diamonds within the migration paths are given at local x maxima for the xz-plane view and y maxima for the yz-plane view, and therefore represent the envelope that contain the revolving motion while drifting motion simultaneously takes place. The final local x maximum and y maximum, which are the global x maximum and y maximum, correspond to when no more outward motion is possible, i.e., the limit cycle, and are marked with filled circles. Unlike the case in a pure revolving motion, the limit cycle now contains a z eccentricity. This method of viewing the migration leads to kinks in the yz-plane view, which are attributed to the distance between the initial position and the first local y maximum.

The inner droplet almost comes into contact with the outer interface in the limit cycle at the y extrema but not at x extrema. This fact is in accordance with Figs. 5(b) and 5(d), and is also revealed when we look at the limit cycle trajectory for various offsets as shown in Fig. 12, as well as from the fact that the final y offsets are larger than the x offsets in Fig. 11.

The outward movement of the inner drop away from the center of the outer drop during the combination of revolving and drifting motions can be contrasted to what may happen to a point

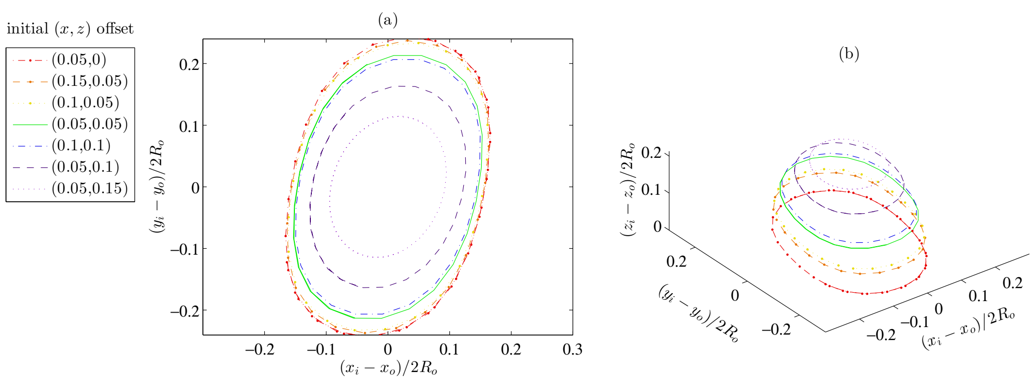

FIG. 12. (a) xy projection and (b) 3D view of the limit cycle movement of the center of the inner droplet with various initial (x,z) offsets noted in the legend. The normalized relative position of inner droplet is plotted for ∼1.5 revolving cycle and shows a tilted elliptical pattern.

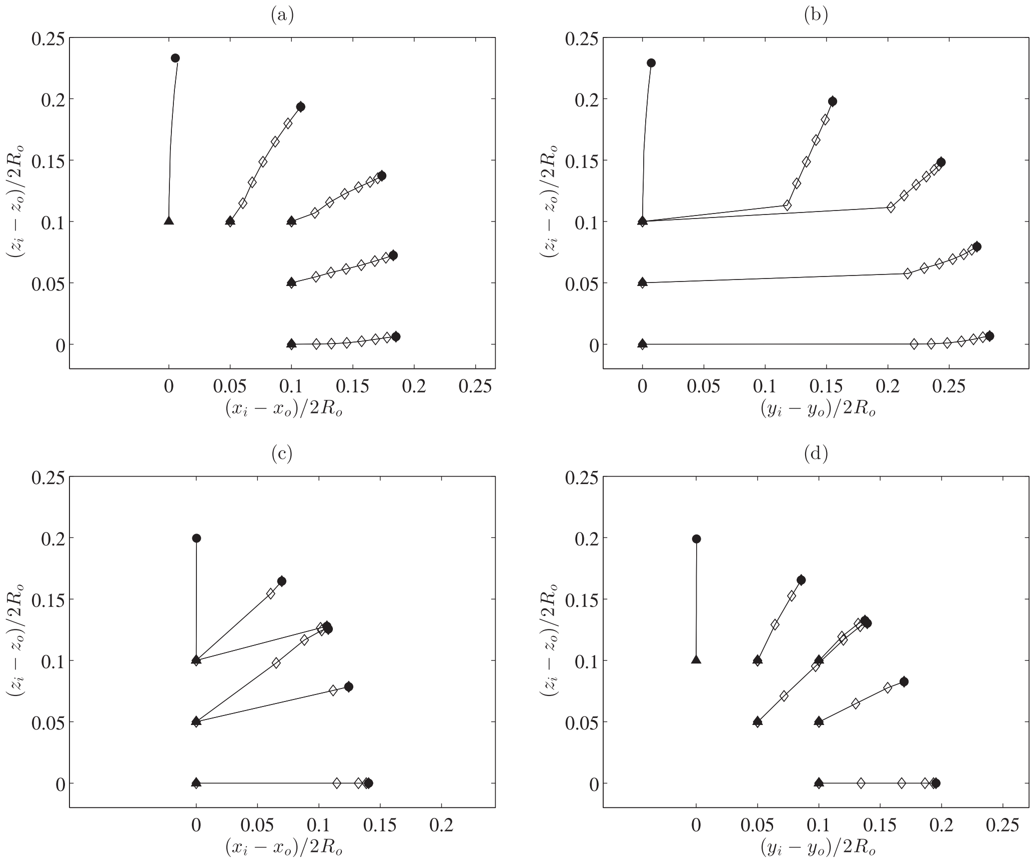

FIG. 13. Behavior of the inner droplet depending on the initial inner droplet placement and the radii ratio. Dimensionless (a) xz-plane view and (b) yz-plane view with the inner droplets initially placed with various (x,z) offsets with $k = 0.4$; dimensionless (c) xz-plane view and (d) yz-plane view with various (y,z) offsets with $k = 0.6$. Filled triangles, filled circles, and open diamonds are used in the manner similar to Fig. 11, and familiar outward migrations to when $k = 0.5$ are observed.

particle in a simple droplet. If the inner drop size were infinitesimal, the streamlines in Fig. 8(a) will be symmetric about the center of the outer drop (which is indeed the case for simple drop), and an outward motion is difficult to imagine. At best, if we imagine the drift movement of many point particles within a simple droplet over time, because the fluid mass has to be conserved inside the said droplet, some point particles will move toward the center of the droplet if some moved outward. On the other hand, when we have an inner droplet of finite size, we see that it only moves outward.

Another characteristic of the droplet migration is that the outward motion in the revolving motion happens with a time scale similar to that of the drifting motion. This is evident because the outward migration paths are approximately radial in Fig. 11. The similarities in the time scales can also be seen from Figs. 5(a), 5(c) and 5(e); as previously stated, the increases in the envelope for relative x and y positions, and the increase in the relative z position, occur over a time scale of $\dot{\gamma} t \sim O(100)$.

B. Effect of radii ratio between inner and outer droplets

As demonstrated in Fig. 13, additional radii ratios of $k = 0.4$ and 0.6 are tested with various offsets. To prove that the outward migration into limit cycle is not dependent upon having the initial eccentricity confined to the xz plane, the inner droplets are placed in the yz plane for the $k = 0.6$

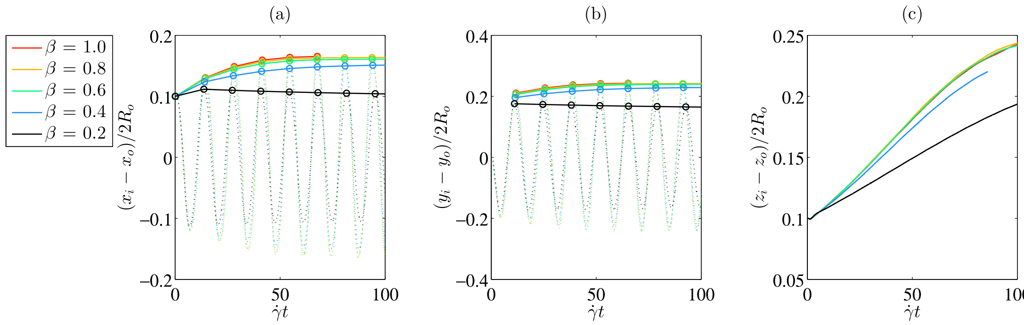

FIG. 14. Dimensionless relative position of the inner droplet vs dimensionless time with various β. Normalized relative (a) x and (b) y positions are shown with dotted lines, with initial inner drop offset in the x direction. The maxima in x and y positions are marked with circles and are connected; (c) normalized relative z position is shown with initial inner drop offset in the z direction.

case. Similar to before, the filled triangles denote the initial positions and the filled circles the global maxima, with open diamonds the local maxima. The lower bound on the radii ratio of $k = 0.4$ is chosen to limit the parasitic current under 1% of the maximum velocity within the computational domain, and the upper bound is chosen to allow the testing of various inner droplet offsets. The radii ratio does not have an impact in the general migration behavior of the inner droplet; the inner droplet migrates such that the eccentricity increases until the limit cycle is reached.

C. Effect of interfacial tension coefficient on migration

The effect of inner interfacial tension on the inner droplet movement is considered. With $k = 0.5$, inner interfacial tension coefficients of $\sigma_i = 0.2$–2.0 are tested, corresponding to $\beta = 0.1$–1 and $\mathrm{Ca}_i = 0.25$–0.025. As shown in Fig. 14, a decrease in β corresponds to a lower migration speed of the inner droplet. Whereas the decrease of β from 1.0 to 0.6 barely affects the overall movement of the inner droplet, the decrease from 0.4 to 0.2 greatly reduces the migration velocities in all the tested cases.

In the case of the revolving motion, a decrease in β from 0.2 to 0.1 results in a reversal in the outward movement. This behavior is similar to that observed in 2D simulations by Hua *et al.*,

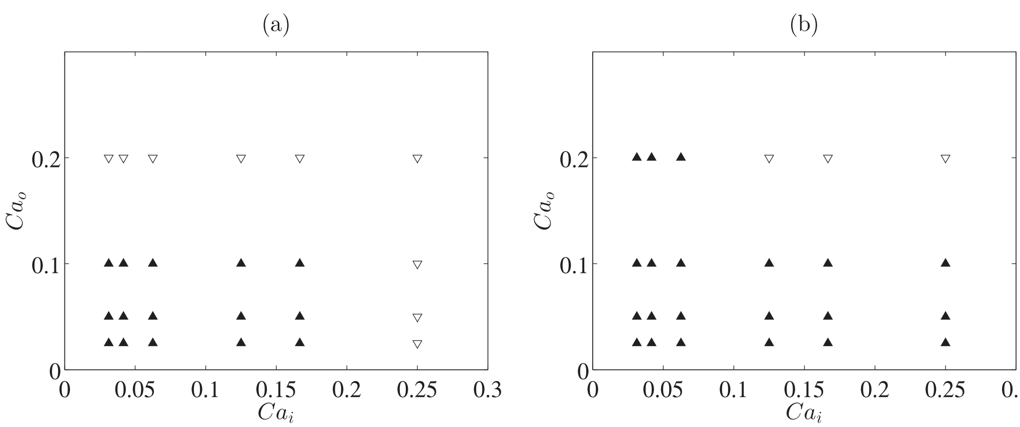

FIG. 15. The increase (filled upward triangle) and decrease (open downward triangle) of eccentricity in the capillary number space with initial (a) x and (b) z eccentricity.

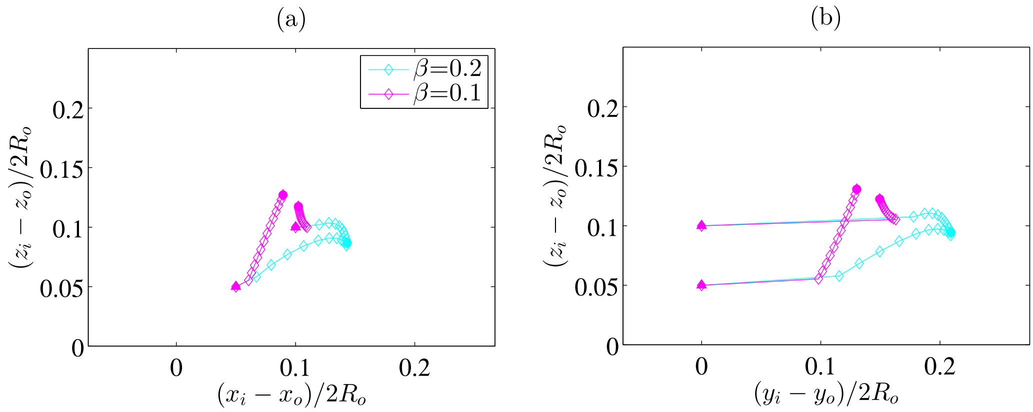

FIG. 16. Comparison between $\beta = 0.1$ and $\beta = 0.2$ with initial (x,z) offsets of (0.05,0.05) and (0.1,0.1) with $\mathrm{Ca}_o = 0.5$. Dimensionless (a) xz-plane view and (b) yz-plane views are shown in identical manner to Figs. 11 and 13. While the inner drop still moves away from the center of the outer droplet, the outward motion is no longer radial.

who chose $\mathrm{Ca}_i = 0.25$ and observed that the inner droplet drifted to the center of the outer droplet regardless of the initial eccentricity.

The drift velocity in the z direction depends weakly on σ_i; there is no reversal in the drift motion with a change in σ_i. Further, a decrease in β from 1 to 0.6 has negligible effect on the drift velocity. It is only when the inner drop deformation grows significantly that the drift velocity noticeably decreases.

When $0.025 < \mathrm{Ca}_o < 0.1$, revolving motion is suppressed when $\mathrm{Ca}_i = 0.25$ but drifting motion is always observed, as shown in Fig. 15; in contrast, when the revolving motion is suppressed for critical $\mathrm{Ca}_i = 0.25$ and $\mathrm{Ca}_o = 0.2$, the drifting motion persists for a wider range of capillary numbers. On top of the effect of capillary numbers, the initial configuration must also be considered: The creation of recirculation zones in Fig. 8(b) does not always occur with an almost-spherical inner drop and initial z asymmetry, and thus even with $\mathrm{Ca}_o = 0.2$, drifting motion can persist. This difference in the critical capillary number at which revolving and drifting motions are suppressed suggests that a more complicated combined motion is possible, where the inner drop may no longer migrate radially outward. For example, when $\beta = 0.1$ and $\mathrm{Ca}_o = 0.05$, the movement of the inner drop is characterized by the suppression of revolving motion, and when $\beta = 0.2$ it is characterized by the suppression of drifting motion depending on the initial configuration. This is shown in Fig. 16.

V. CONCLUSION

We numerically investigated the temporal evolution of eccentric compound droplets subject to a simple shear flow with equal viscosities and densities in all phases. When the eccentricity is confined within the plane of shear, a revolving motion is observed for the inner droplet. Throughout the revolving motion, the inner droplet orbits about and slowly migrates away from the center of the outer droplet until only a thin film of liquid remains between the inner and outer interfaces, at which point the inner droplet revolves about the periphery of the outer interface in a limit cycle behavior. When the eccentricity is normal to the plane of shear, a drifting motion is observed, where the inner drop moves perpendicularly to the plane of shear, slowly increasing the eccentricity. The time scale relevant to the drifting motion is similar to that of the outward motion in the revolving motion.

Revolving and drifting motions increase the eccentricity of the compound droplet when $\mathrm{Re} \leqslant 5$, $\mathrm{Ca}_o \leqslant 0.1$, and $\mathrm{Ca}_i < 0.1$ and are not affected by k in the range 0.4–0.6. Because simple shear flows are ubiquitous and easy to reproduce, and because they form the basis of linearized analysis of more complicated flows, this research sheds a light onto understanding the temporal evolution and eccentric breakup mechanism of compound droplets.

---

[1] F. Leal-Calderon, J. Bibette, and V. Schmitt, Double emulsions, in *Emulsion Science: Basic Principles* (Springer, New York, 2007), pp. 173–199.
[2] R. E. Johnson and S. S. Sadhal, Fluid mechanics of compound multiphase drops and bubbles, Annu. Rev. Fluid Mech. **17**, 289 (1985).
[3] H.-C. Kan, H. S. Udaykumar, W. Shyy, and R. Tran-Son-Tay, Hydrodynamics of a compound drop with application to leukocyte modeling, Phys. Fluids **10**, 760 (1998).
[4] J. M. Rallison, The deformation of small viscous drops and bubbles in shear flows, Annu. R. Fluid Mech. **16**, 45 (1984).
[5] P. C.-H. Chan and L. G. Leal, The motion of a deformable drop in a second-order fluid, J. Fluid Mech. **92**, 131 (1979).
[6] M. Shapira and S. Haber, Low Reynolds number motion of a droplet in shear flow including wall effects, Int. J. Multiphase Flow **16**, 305 (1990).
[7] H. A. Stone, Dynamics of drop deformation and breakup in viscous fluids, Ann. Rev. Fluid Mech. **26**, 65 (1994).
[8] K. S. Chang and W. L. Olbricht, Experimental studies of the deformation and breakup of a synthetic capsule in steady and unsteady simple shear flow, J. Fluid Mech. **250**, 609 (1993).
[9] M. T. Sullivan and H. A. Stone, The role of feedback in microfluidic flow-focusing devices, Phil. Trans. R. Soc. London, Ser. A **366**, 2131 (2008).
[10] J. K. Klahn, J. J. M. Janssen, G. E. J. Vaessen, R. de Swart, and W. G. M. Agterof, On the escape process during phase inversion of an emulsion, Colloids Surf., A **210**, 167 (2002).
[11] S. S. Sadhal and H. N. Oguz, Stokes flow past compound multiphase drops: The case of completely engulfed drops/bubbles, J. Fluid Mech. **160**, 511 (1985).
[12] S. Torza and S. G. Mason, Three-phase interactions in shear and electrical fields, J. Colloid Interface Sci. **33**, 67 (1970).
[13] Y. Chen, X. Liu, and M. Shi, Hydrodynamics of double emulsion droplet in shear flow, Appl. Phys. Lett. **102**, 051609 (2013).
[14] Y. Chen, X. Liu, and Y. Zhao, Deformation dynamics of double emulsion droplet under shear, Appl. Phys. Lett. **106**, 141601 (2015).
[15] Y. Chen, X. Liu, C. Zhang, and Y. Zhao, Enhancing and suppressing effects of an inner droplet on deformation of a double emulsion droplet under shear, Lab Chip **15**, 1255 (2015).
[16] H. Hua, J. Shin, and J. Kim, Dynamics of a compound droplet in shear flow, Int. J. Heat Fluid Flow **50**, 63 (2014).
[17] S. Patlazhan, S. Vagner, and I. Kravchenko, Steady-state deformation behavior of confined composite droplets under shear flow, Phys. Rev. E **91**, 063002 (2015).
[18] K. A. Smith, J. M. Ottino, and M. Olvera de la Cruz, Encapsulated Drop Breakup in Shear Flow, Phys. Rev. Lett. **93**, 204501 (2004).
[19] H. Lamb, *Hydrodynamics* (Dover, New York, 1945), pp. 594–599.
[20] G. I. Taylor, The viscosity of a fluid containing small drops of another fluid, Proc. R. Soc. London, Ser. A **138**, 41 (1932).
[21] R. G. Cox, The deformation of a drop in a general time-dependent fluid flow, J. Fluid Mech. **37**, 601 (1969).
[22] H. A. Stone and L. G. Leal, Breakup of concentric double emulsion droplets in linear flows, J. Fluid Mech. **211**, 123 (1990).
[23] X. Qu and Y. Wang, Dynamics of concentric and eccentric compound droplets suspended in extensional flows, Phys. Fluids **24**, 123302 (2012).

[24] Y. Song, J. Xu, and Y. Yang, Stokes flow past a compound drop in a circular tube, Phys. Fluids **22**, 072003 (2010).

[25] S. Mandal, U. Ghosh, and S. Chakraborty, Effect of surfactant on motion and deformation of compound droplets in arbitrary unbounded stokes flows, J. Fluid Mech. **803**, 200 (2016).

[26] H. Haj-Hariri, A. Nadim, and A. Borhan, Recriprocal theorem for concentric compound drops in arbitrary stokes flows, J. Fluid Mech. **252**, 265 (1993).

[27] P. G. Saffman, The lift on a small sphere in a slow shear flow, J. Fluid Mech. **22**, 385 (1965).

[28] S. Dabiri, J. Lu, and G. Tryggvason, Transition between regimes of a vertical channel bubbly upflow due to bubble deformability, Phys. Fluids **25**, 102110 (2013).

[29] B. Bunner and G. Tryggvason, Effect of bubble deformation on the properties of bubbly flows, J. Fluid Mech. **495**, 77 (2003).

[30] G. I. Taylor, The formation of emulsions in definable fields of flow, Proc. R. Soc. London, Ser. A **146**, 501 (1934).

[31] T. Hayase, J. A. C. Humphrey, and R. Greif, A consistently formulated QUICK scheme for fast and stable convergence using finite-volume iterative calculation procedures, J. Comput. Phys. **98**, 108 (1992).

[32] A. J. Chorin, Numerical solution of the Navier-Stokes equations, Math. Comp. **22**, 745 (1968).

[33] R. D. Falgout and U. M. Yang, hypre: A library of high performance preconditioners, in *Computational Science—ICCS 2002: International Conference Amsterdam, The Netherlands, April 21–24, 2002 Proceedings, Part III*, edited by P. M. A. Sloot, A. G. Hoekstra, C. J. K. Tan, and J. J. Dongarra (Springer, Berlin, 2002), pp. 632–641.

[34] S. O. Unverdi and G. Tryggvason, A front-tracking method for viscous, incompressible, multi-fluid flows, J. Comput. Phys. **100**, 25 (1992).

[35] J. W. Ha, Y. Yoon, and L. G. Leal, The effect of compatibilizer on the coalescence of two drops in flow, Phys. Fluids **15**, 849 (2003).

[36] F. D. Rumscheidt and S. G. Mason, Particle motions in sheared suspensions XII: Deformation and burst of fluid drops in shear and hyperbolic flow, J. Colloid Sci. **16**, 238 (1961).

[37] S. K. Veerapaneni, Y.-N. Young, P. M. Vlahovska, and J. Bławzdziewicz, Dynamics of a Compound Vesicle in Shear Flow, Phys. Rev. Lett. **106**, 158103 (2011).

[38] C. Zhou, P. Yue, and J. J. Feng, Deformation of a compound drop through a contraction in a pressure-driven pipe flow, Int. J. Multiphase Flow **34**, 102 (2008).